Phonons in silver gallium diselenide

1997 J. Phys.: Condens. Matter 9 6579

(http://iopscience.iop.org/0953-8984/9/31/011)

J. Phys.: Condens. Matter **9** (1997) 6579–6589. Printed in the UK PII: S0953-8984(97)79984-3

Phonons in silver gallium diselenide

R Fouret†, P Derollez†, A Laamyem†, B Hennion‡ and J Gonzalez§

† Laboratoire de Dynamique et Structure des Matériaux Moléculaires, Université de Lille I, 59655 Villeneuve d'Ascq Cédex, France

‡ Laboratoire Léon Brillouin, Centre d'Etudes Nucléaires de Saclay, 91191 Gif sur Yvette, France

§ Centro de Estudios de Semiconductores, Facultad de Ciencias, Universidad de Los Andes, Merida 5101, Venezuela

Received 2 December 1996

Abstract. The dispersion curves along the directions [100] and [001] of $AgGaSe_2$ have been measured by inelastic neutron scattering. The results are analysed with different rigid-ion models: Born–von Karman and valence force field models, which give a good agreement with experiments. Additional measurements of the acoustical branches allow us to determine elastic stiffness constants which are ($\times 10^{10}$ N m^{-2}) $c_{11} = 8.01$, $c_{33} = 7.07$, $c_{44} = 2.12$, $c_{66} = 2.47$, $c_{12} = 5.16$, $c_{13} = 5.26$. The compressibility calculated from these constants is in accordance with the experimental value.

1. Introduction

Silver gallium diselenide $AgGaSe_2$ is a I–III–VI_2 direct energy gap semiconductor ($E_g \sim 1.79$ eV at 300 K) compound that crystallizes in the tetragonal chalcopyrite (spatial group $I\bar{4}2d$) structure and its isoelectronic cubic analogue is $Zn_{0.5}Cd_{0.5}Se$. The replacement of the cationic sublattice by two different atomic species induced (i) a tetragonal distortion, usually a compression, with $\varepsilon = 2 - c/a \neq 0$ and (ii) anion displacements to non-cubic positions characterized by the parameter $u = 0.25 + (d^2_{I-VI} - d^2_{III-VI})/a^2$. The primitive cell includes eight atoms whose fractional coordinates are given in table 1 [1].

Table 1. Fractional coordinates of the atoms in the primitive cell.

Ag1	0	0	0
Ag2	$\frac{1}{2}$	0	$-\frac{1}{4}$
Ga1	0	$-\frac{1}{2}$	$-\frac{1}{4}$
Ga2	$\frac{1}{2}$	$-\frac{1}{2}$	0
Se1	$-\frac{1}{4}$	u	$-\frac{1}{8}$
Se2	$-u$	$-\frac{1}{4}$	$\frac{1}{8}$
Se3	u	$\frac{1}{4}$	$\frac{1}{8}$
Se4	$\frac{1}{4}$	$-u$	$-\frac{1}{8}$

The lattice parameters at 300 K are $a = 5.992$ Å, $c = 10.888$ Å and $c/a = 1.817$ [1–3]. Two values are found in the literature for the u parameter, $u = 0.27$ and $u = 0.298$ [4].

0953-8984/97/316579+11$19.50

This material has been shown to be potentially useful in non-linear optics [5–7] because of its highly non-linear coefficients, wide transparency range (from 0.7–17 μm) and its ability to be phase matched over a large part of that range.

The following properties seem anomalous in $AgGaSe_2$ as compared with Cu–III–VI_2 semiconductors. (i) In the Cu compounds the linear thermal expansion coefficients α_a and α_c are always positive at 300 K and $\alpha_a < \alpha_c$. In the Ag compounds α_c is negative [8] for a temperature higher than about 100 K. (ii) In the Cu compounds the isothermal compressibility $\chi_a > \chi_c$, while in $AgGaSe_2$ the c parameter is more compressible than the a parameter [9, 10]. (iii) Under pressure, Raman [12, 13], optical [14] and x-ray studies [10] have shown that $AgGaSe_2$ undergoes a phase transition to an orthorhombic-like structure at about 5 GPa. In the case of $CuGaSe_2$ the phase transition to an NaCl-type structure is observed at 13 GPa. Therefore the stability range of the chalcopyrite phase is much smaller in $AgGaSe_2$. Evidence is rising that the stability of the chalcopyrite phase is associated with the softening of the transverse acoustic (TA) phonon modes [15] and also with the low-frequency optical modes ($\Gamma_5 = 26$ cm^{-1} in $AgGaSe_2$ at 77 K) [16, 17].

The knowledge of the lattice dynamics of this compound, and particularly of the acoustic and the low-energy optical modes, should improve the understanding of these properties. Therefore inelastic neutron scattering measurements have been carried out on a single crystal of $AgGaSe_2$ to determine the phonon dispersion curves at room temperature in the main symmetry directions. The obtained results are reported in section 2. The experimental data allowed us to model the lattice dynamics. The Born–von Karman (BvK) model and the valence force field (VFF) model are presented in section 3. In section 4 from the acoustical branches we deduce the elastic constants and the compressibility. The discussion and the concluding remarks are developed in sections 5 and 6.

2. Experimental results

The sample, produced by the vertical Bridgman technique, had a volume of about 0.3 cm^3. Inelastic neutron scattering experiments have been carried out at room temperature and atmospheric pressure at the Orphée reactor at the Laboratoire Léon Brillouin on the triple-axis spectrometer 1T installed on a thermal source. The monochromator and the analyser were pyrolytic graphite in (002) reflection. The measurements were performed at constant $k_F = 2.6623$ Å^{-1} with a graphite filter after the sample to prevent higher-order contamination. The horizontal collimations were 30′–40′–40′–40′ yielding a FWHM energy resolution of 0.2 THz for zero energy transfer. The experimental conditions have been chosen in order to obtain the optimum between the resolution and the signal intensity: the dynamical structure factor calculations allow us to choose the best Brillouin zone for the selected branch.

The phonon branches have been measured in the whole energy range in the [001] and [100] directions. The acoustic branches have also been measured along [110], [101] and [111] in order to obtain a complete determination of the elastic constants. The data have been systematically corrected from instrumental resolution effect.

The main experimental difficulty is related to the number of branches. There are eight atoms in the primitive cell, therefore 24 phonon branches in a general direction. Only in the [001] direction is this number reduced to 17: the irreducible decomposition is then $5\Lambda_1+5\Lambda_2+7\Lambda_3$ where the Λ_3 modes are doubly degenerate. In order to label the observed modes and to have some predictions on the most favourable Brillouin zone to measure a given mode, we have used a group theoretical analysis and a rough BvK model with the force constants given by Artus *et al* [18]. This has been done with the use of the Unisoft

program package [19] and was of a great help to disentangle the observed modes. For the phonons which have very close frequencies, the assignment of the dispersion curves may be made difficult by many crossings of the modes and, in the Brillouin zone used, the fast variation of the dynamical structure factor versus the wave vector q along the given direction. This behaviour, if we are not careful, entails mistakes in the attribution of phonons to the different branches. The results obtained in the [001] and [100] directions are shown in figures 1 and 2 respectively.

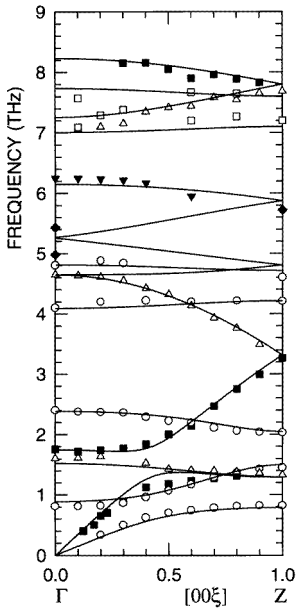

Figure 1. Dispersion curves of phonons along the [001] direction. The points correspond to the neutron measurements, the full lines to the BvK model.

3. Dynamical models

3.1. Born–von Karman model

The first model to analyse the experimental data is a Born–von Karman (BvK) model including short-range forces and electrostatic forces. The term of the dynamical matrix corresponding to Coulomb forces is calculated following the Ewald summation method. Short-range forces have been assumed to be central forces and their contribution to the dynamical matrix is then written as

$$\Phi(lK\alpha, l'k'\beta) = -(L-T)\frac{r_\alpha r_\beta}{r^2} - T\delta_{\alpha\beta}. \tag{1}$$

L and T are the 'longitudinal' and the 'tranverse' force constants, given by

$$L_{lk,l'k'} = \left.\frac{\mathrm{d}^2\Phi(lk,l'k')}{\mathrm{d}r^2}\right|_{r=|\boldsymbol{x}(lk)-\boldsymbol{x}(l'k')|} \qquad T_{lk,l'k'} = \left.\frac{1}{r}\frac{\mathrm{d}\Phi(lk,l'k')}{\mathrm{d}r}\right|_{r=|\boldsymbol{x}(lk)-\boldsymbol{x}(l'k')|} \tag{2}$$

where $\boldsymbol{r} = \boldsymbol{x}(lk) - \boldsymbol{x}(l'k')$, $r = |\boldsymbol{r}|$; $\boldsymbol{x}(lk)$ and $\boldsymbol{x}(l'k')$ are the equilibrium positions of the atoms lk and $l'k'$, and $\Phi(lk, l'k')$ is the interaction potential between lk and $l'k'$. As the

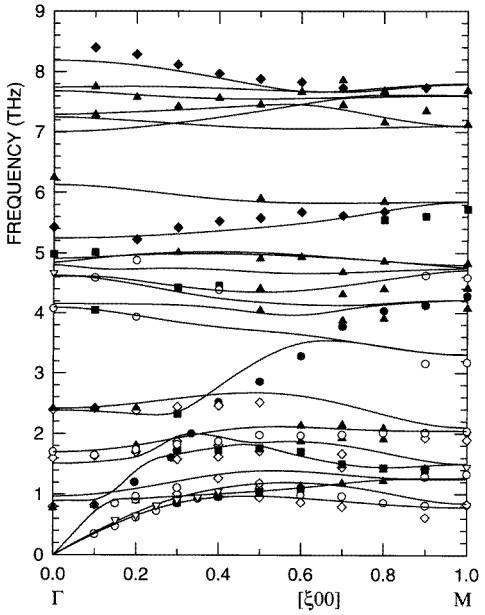

Figure 2. Dispersion curves of phonons along the [100] direction. The points correspond to the neutron measurements; in particular, the experimental points of the longitudinal acoustic branch are represented on this figure by the points •. The full lines correspond to the BvK model.

atomic equilibrium positions correspond to a minimum of the potential energy, the net forces on any atom must vanish. This is ensured by symmetry for silver and gallium atoms which are located on $\bar{4}$ axes, but for the selenium atoms this implies the following constraint:

$$\sum_{l'k'} r_\alpha T_{lk,l'k'} + q_k E_\alpha(lk) = 0. \tag{3}$$

We have taken into account force constants up to an extent of 5.5 Å. This corresponds mainly to the first and the second neighbours for the interactions Ag1–Se1, Ga1–Se1, Se1–Se2 and Se1–Se4. In order to avoid the multiplicity of adjustable parameters, we kept the same values for equivalent pairs with slightly different distances, as seen in table 2.

The force constants have been adjusted using the Unisoft program [19] to obtain the best fit to the measured data. We used about 60 measured frequencies: the zone centre values, the zone boundary values in the [100] and [001] directions and some values measured at $[0.5, 0, 0]$ and $[0, 0, 0.5]$. The obtained agreement is fairly good, as seen in figures 1 and 2 where experimental and calculated values are reported. The corresponding force constants are reported in table 2, together with the effective charges. The standard deviations for the force constants L and T of the preponderant Ag1–Se1 and Ga1–Se1 interactions are about 5%; the other parameters are less well defined. The fit was found to be sensitive to the u parameter, and the best reliability factor of 2% was obtained for $u = 0.29$.

In figure 3, we show also the phonon density of states calculated from the force constants obtained by the previous fit with $u = 0.29$. As observed there are three frequency ranges which are in good agreement with the dispersion curves of figures 1 and 2.

Table 2. Atomic force constants for the interactions considered.

$Z_{Ag} = 0.53$	$Z_{Ga} = 0.93$	$Z_{Se} = -0.73$	
Interaction	Shell radius (Å)	L (N m^{-1})	T (N m^{-1})
Ag1–Se1	2.67	55.5	−9.7
	4.53	3.3	0.5
	4.71	3.3	0.5
	5.01	3.3	0.5
Ga1–Se1	2.38	117.1	−5.1
	4.68	1.9	1.7
	4.86	1.9	1.7
	5.15	1.9	1.7
Ag1–Ag2	4.05	0.2	−1.2
Ag1–Ga1	4.05	−1.6	−0.3
Ag1–Ga2	4.24	−1.6	−0.3
	5.44	0.0	−1.8
Ga1–Ga2	4.05	9.0	0.9
Se1–Se2	3.88	6.0	−2.0
	4.24	7.0	0.0
Se1–Se4	3.91	6.0	−2.0
	4.59	7.0	0.0

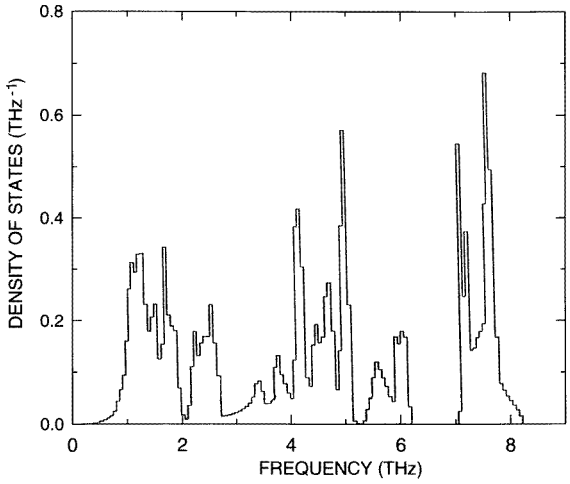

Figure 3. The phonon density of states of $AgGaSe_2$ with $u = 0.29$.

3.2. The valence force-field (VFF) model

A more realistic description of the short-range valence forces in tetrahedrally coordinated crystals is the VFF model, where interatomic forces are described through bond stretching and angular bond bending forces. In heteropolar structures such as chalcopyrites we add Coulomb forces described by point charges on the atom sites. In the simplified Keating model [25] the bond stretching potential energy is given, in the harmonic approximation, by

$$V_b(i, j) = \tfrac{1}{2}\alpha(\boldsymbol{n}_{ij} \cdot \boldsymbol{u}_{ij})^2 \tag{4}$$

for the (i, j) bond: $\boldsymbol{n}_{ij}$ is the unit vector along this bond; $\boldsymbol{u}_{ij} = \boldsymbol{u}_i - \boldsymbol{u}_j$, $\boldsymbol{u}_i$ and $\boldsymbol{u}_j$ being the displacements of the atoms i and j. Here, we denote by α_1 the stretching constant for the Ag–Se bond and by α_2 that for the Ga–Se bond. The bond bending potential energy may be written

$$V_{bb}(i, j, k) = \tfrac{1}{2}\beta(\boldsymbol{n}_{ji} \cdot \boldsymbol{u}_{jk} + \boldsymbol{n}_{jk} \cdot \boldsymbol{u}_{ji})^2. \tag{5}$$

The five parameters β with their meanings are shown in table 3.

Table 3. Bond stretching and bond bending potential parameters.

$Z_{Ag} = 0.53$	$Z_{Ga} = 0.93$	$Z_{Se} = -0.73$
Type of bond	Bond constant	Fitted values (N m^{-1})
Ag–Se	α_1	56.3
Ga–Se	α_2	120.6
Se–Ag–Se	β_1	0.2
Se–Ga–Se	β'_1	−1.3
Ag–Se–Ga	β_2	0.6
Ag–Se–Ag	β_3	−3.7
Ga–Se–Ga	β'_3	−7.0

Using this model the fit yielded a reliability factor of about 5%. This is not as good as the BvK model, but is obtained with seven adjustable parameters instead of 20 (see tables 2 and 3). Adding interactions between atoms which are not linked such as Ag1–Ga1 and Se1–Se4 gives results quite similar to the BvK ones (reliability factor of 2% and analogous standard deviations for the parameters).

Both models give a good agreement with the neutron measurements. In table 4 are reported Raman frequencies measured at 77 K and neutron values obtained at 300 K at the Γ point.

Table 4. Neutron frequencies and Raman frequencies [16] at the Γ point. The symbol * denotes an extrapolated value.

Symmetry	Neutron freq. (THz) at 300 K	Raman freq. (THz) at 77 K
A1		5.43
A2	4.68	
	6.25	
E	0.81	0.81 (T)
	2.40	2.52 ($L + T$)
	4.10	4.11 (T) 4.14 (L)
	4.80	4.86 (T) 4.95 (L)
	7.10*	7.64 (T)
	7.60*	7.52 (T) 8.30 (L)
B1	1.62	1.74
	4.68	4.80
	7.10	7.58
B2	1.76	1.74 ($T + L$)
	4.95	4.65 (T) 4.83 (L)
	8.20*	7.55 (T) 8.24 (L)

4. Elastic constants and compressibility

The measurement of the phonon acoustic modes at small q values gives the possibility of determining the sound velocity in various directions, and hence of determining the elastic constants. Figure 4 shows a comparison between the experimental acoustic dispersion curves in the [111] direction and those obtained by the BvK model, where we can see a rather good coincidence between measured and calculated branches, in particular for the longitudinal mode. The $\boldsymbol{q}$ range accessible with neutron scattering is such that departure from the linear dependence has to be accounted for. This has been done by writing $2\pi\nu = qV(q)$ with $V(q) = V(0)(1 - hq^2)$ and is illustrated in figure 5 for a transverse mode TA_2 along the [100] direction. Such a determination has been performed on 14 acoustic branches and the results are reported in table 5. To extract the elastic stiffness constants, we have to take into account that $AgGaSe_2$ is piezoelectric. The velocity is then given by

$$\left[\rho V^2\delta_{\alpha\beta} - \left(\Gamma_{\alpha\beta} + \frac{\gamma_\alpha\gamma_\beta}{\varepsilon}\right)\right]u_\beta = 0 \tag{6a}$$

where

$$\Gamma_{\alpha\beta} = c_{\alpha\beta\gamma\delta}n_\gamma n_\delta \qquad \gamma_\alpha = e_{\gamma\alpha\delta}n_\gamma n_\delta \tag{6b}$$

$$\varepsilon = \varepsilon_{\gamma\delta}n_\gamma n_\delta \tag{6c}$$

and $c_{\alpha\gamma\beta\delta}$, $e_{\gamma\alpha\delta}$ and $\varepsilon_{\gamma\delta}$, are respectively the elastic stiffness constants, the piezoelectric constants ($e_{i\alpha\beta} = d_{i\gamma\delta}c_{\gamma\delta\alpha\beta}$) and the dielectric constants; n_α is the component along Ox_α of the unit vector along the propagation direction.

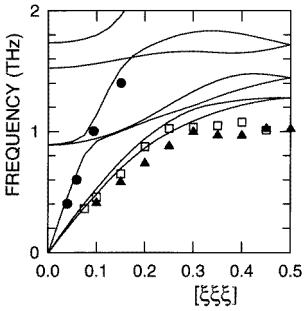

Figure 4. Experimental acoustic dispersion curves in the [111] direction. The full lines correspond to the BvK model.

The calculation shows that the velocities along the [100] and [001] directions are independent of the piezoelectric constants. For the other directions of propagation the piezoelectric constants introduce a corrective term to the propagation velocities. For example, in the [110] direction, the transverse mode polarized along the [001] direction has a velocity V_{T_2} such that

$$V_{T_2}^2 = \frac{1}{\rho}\left(c_{44} + \frac{e_{14}^2}{\varepsilon_{11}}\right). \tag{7}$$

This explains (cf table 5) the difference between the TA_2 [100] and the TA_2 [110] branches, which both involve the c_{44} elastic constant but where only the [110] modes involves also the piezoelectric constant.

Due to the tetragonal structure of the crystal, there are six elastic constants and two piezoelectric coefficients. Unfortunately, even with our 14 experimental values the

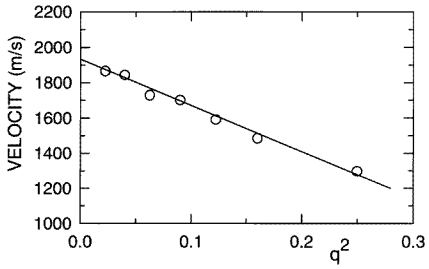

Figure 5. An illustrative example of the calculation of the phonon velocity of the transverse mode TA_2 along the [100] direction.

Table 5. Experimentally extrapolated and calculated velocities of acoustic phonon modes with different polarization vectors in $AgGaSe_2$.

Phonon mode	Polarization vector	$V(0)$ (m s^{-1}) experimental	V (m s^{-1}) calculated
LA [100]	[100]	3720	3748
TA_1 [100]	[010]	2093	2081
TA_2 [100]	[001]	1932	1930
LA [110]	[110]	3971	3986
TA_1 [110]	$[1\bar{1}0]$	1589	1579
TA_2 [110]	[001]	2069	2075
LA [001]	[001]	3514	3521
TA [001]	[100]	1919	1930
LA [101]	$[10v]$	3875	3862
TA_1 [101]	$[10 - v^{-1}]$	1586	1574
TA_2 [101]	[010]	2066	2092
LA [111]	$[11w]$	4080	4041
TA_1 [111]	$[11w - 2w^{-1}]$	1834	1828
TA_2 [111]	$[\bar{1}10]$	1625	1629

refinement does not yield a reliable determination of the piezoelectric constants. So we have used the values given by Horinaka [27] which correspond to the three non-zero elements of the piezoelectric tensor, namely $d_{14} = d_{24} = 9.0 \times 10^{-12}$ C N^{-1} and $d_{36} = 3.7 \times 10^{-12}$ C N^{-1}. Refining then, we obtain the elastic constant values reported in table 6. The standard deviation from the least-square fit is within 2% and it can be seen that the Born stability criteria for the tetragonal chalcopyrite structure [29] are satisfied by the obtained c_{ij}. Calculated velocities in the direction corresponding to experiments are reported in table 5. We may also use the relations between the elastic compliances given by Horinaka *et al* [27]: $sp_1 = \frac{1}{4}(s_{11}+2s_{13}+s_{33}+s_{44})$ and $sp_2 = \frac{1}{4}(2s_{11}+2s_{12}+s_{66})$. Using our data we obtain $sp_1 = 2.03 \times 10^{-11}$ m^2 N^{-1} and $sp_2 = 1.95 \times 10^{-11}$ m^2 N^{-1}, in very good agreement with the values of $sp_1 = 2.10 \times 10^{-11}$ m^2 N^{-1} and $sp_2 = 1.99 \times 10^{-11}$ m^2 N^{-1} of Horinaka, as deduced from their measurements of the piezoelectric coefficients by a self-resonance method.

For comparison the values of the elastic constants obtained by ultrasonic measurements [30] in $AgGaSe_2$ are also shown. As observed the agreement is not satisfying. We also present the values of the elastic constants of $AgGaS_2$ [28]. Our values, in very good concordance with the values for $AgGaS_2$ and also with the relations reported by Horinaka [27], lead us to think that a mistake has been probably made in the determination of the

Table 6. Elastic constants of $AgGaSe_2$ from our neutron experiments. The values of $AgGaSe_2$ and $AgGaS_2$ obtained by ultrasonic measurements [30] and Brillouin scattering [28] respectively are also given. Elastic constants are in units of 10^{10} Newtons per square metre.

Elastic constant	$AgGaSe_2$[a]	$AgGaSe_2$[b]	$AgGaS_2$[c]
c_{11}	8.01 ± 0.05	8.98	8.79 ± 0.05
c_{33}	7.07 ± 0.07	5.80	7.58 ± 0.05
c_{44}	2.12 ± 0.03	2.17	2.41 ± 0.05
c_{66}	2.47 ± 0.03	1.33	3.08 ± 0.05
c_{12}	5.16 ± 0.06	6.57	5.48 ± 0.05
c_{13}	5.26 ± 0.08	4.51	5.92 ± 0.06

[a] Our result.
[b] [30].
[c] [28].

elastic constants by ultrasonic measurements [30].

On the other hand, we may use the linear elasticity approximation [29] to calculate the compressibility from the elastic constants. We may write

$$\chi_T = \chi_{T,c} + 2\chi_{T,ab} \tag{8}$$

where $\chi_{T,c}$ and $\chi_{T,ab}$ are the compressibilities along the c axis and in the ab plane respectively of the chalcopyrite structure. These two compressibilities are expressed as

$$\chi_{T,c} = \frac{c_{11} + c_{12} - 2c_{13}}{c} \tag{9}$$

$$\chi_{T,ab} = \frac{c_{33} - c_{13}}{c} \tag{10}$$

where

$$c = c_{33}(c_{11} + c_{12}) - 2c_{13}^2.$$

From our elastic constants we obtain $\chi_{T,c} = 7.32 \times 10^{-3}$ GPa^{-1} and $\chi_{T,ab} = 4.7 \times 10^{-3}$ GPa^{-1}, hence $\chi_T = 1.67 \times 10^{-2}$ GPa^{-1} and for the bulk modulus $B_T = 1/\chi_T = 60$ GPa. This value agrees very well with the value $B_T = 65$ GPa reported in [10] from *in situ* x-ray measurements under pressure on $AgGaSe_2$ at 300 K.

5. Discussion

We have seen that our inelastic neutron scattering measurements are in very good agreement with previous Raman and infrared measurements on zone centre frequencies [16, 18], but, now, the knowledge of the dispersion curves allows us to obtain a more reliable model than previous approaches of the lattice dynamics of chalcopyrites based only on infrared and Raman measurements. For instance, Artus *et al* used a Keating model with only four force constants, namely α_1, α_2, β_1 and β_1', but neglected Coulomb forces. Koschel and Bettini used the same Keating model with four force constants and the Coulomb forces to interpret infrared and Raman measurements on the S chalcopyrite family, but they obtain a reasonable agreement only for frequencies higher than 190 cm^{-1}. Lauwers and Harman [32] obtained a good fit of his 13 experimental data but with a Urey–Bradley model including nine parameters. Only the dispersion curves calculated by Poplavnoi and Tjutarev [31] have a qualitative similarity with the dispersion curves that we have measured.

The only common conclusion is the relative values obtained for the stretching constants α_{GaSe} and α_{AgSe}, which are found in a 2:1 ratio, as by Artus *et al* [18]. However, their absolute values differ when passing from our model to the Artus model (respectively $\alpha_{AgSe} = 55.5(18.65)$ and $\alpha_{GaSe} = 117.1(34.82)$). The difference is essentially due to the introduction in our calculation of the electrostatic forces. This previous ratio is in agreement with the compressibility values of the I–VI and III–VI bonds obtained by single-crystal x-ray diffraction and EXAFS measurements under pressure, in particular for the values of $CuGaS_2$ [24] and $AgGaSe_2$ [10].

The measured acoustic dispersion curves of $AgGaSe_2$ are quite similar to those that have been measured by neutron scattering experiments on binary ZnS, ZnSe, ZnTe and CdSe of the II–VI family [21], particularly the TA [100] mode. In these binary compounds the TA(X) or TA(L) mode softens under pressure, yielding a negative Grüneisen constant. In I–III–VI_2 chalcopyrite semiconductors negative values of the expansion coefficient $\alpha(T)$ have been reported for temperatures lower than 80 K [23]. The TA [100] phonon with $\nu = 24.3$ cm^{-1} is probably responsible for that behaviour and should be seen to soften with decreasing temperature or increasing pressure. Further neutron scattering experiments are planned to obtain more information on that point.

Even in the absence of direct measurements of mode softening under pressure, which might be difficult to realize with neutron experiments, the model of the lattice dynamics that we have obtained with the ambient pressure determination of the phonon spectrum should allow us to clarify the question of the chalcopyrite structure stability. Indeed, infrared and Raman measurements under pressure would be sufficient to obtain the first derivatives of the pressure dependence of the force constants. Injecting these modified force constants into our model would then point out the modes involved in the phase transition.

6. Concluding remarks

We have determined from inelastic neutron scattering at 300 K the dispersion curves of acoustic and optical phonons in $AgGaSe_2$. These dispersion curves have been compared with different rigid-ion models which differ in the representation of the short range forces: the Born–von Karman (BvK) model and the valence force field (VFF) model. The following conclusions can sum up the results of this work.

(i) As in the II–VI semiconductors, the characteristic features of the lattice dynamics of $AgGaSe_2$ are that the TA phonon mode frequencies are rather low lying and have a very flat dispersion at large wave vectors, which could be a hint that the pressure induced instability is correlated to the softness of the TA phonon modes.

(ii) Using the BvK model we obtain a good agreement between the fitted and the experimental dispersion curves. From this result we see that the stretching force constant value for the Ag–Se bond is approximately half of the stretching force constant for the Ga–Se bond. This result is in agreement with the results of [24], where pressure experiments on $CuGaSe_2$ shows that the Cu–S bond is softer than the Ga–S bond.

(iii) The elastic constants of $AgGaS_2$ are not very different from the values for $AgGaSe_2$ and the shear modulus $\frac{1}{2}(c_{11} - c_{12})$ is comparable and relatively small in both materials; these are in good agreement with the relations given by Horinaka, which have been obtained by a method of electric resonance.

(iv) The quality of the model based now on a large set of experimental data including neutron and optical measurements gives us great hope of being able to explain the temperature dependence of the dilatation and the mechanism of the crystal instability of this compound using the pressure dependence of Raman and IR frequencies.

Acknowledgments

The authors wish to thank Dr G Eckold who provided the program package Unisoft. One of us (JG) acknowledges the CEFI-PCP (France) and the CONICIT-Materials (Venezuela). This work was performed under the frame work of EEC contract No CI1-CT94-0031.

The Laboratoire de Dynamique et Structure des Matériaux Molécularies is Unité Associée au CNRS No 801.

References

[1] Shay L and Wernick J H 1975 *Ternary Chalcopyrite Semiconductors: Growth, Electronic Properties and Applications* (New York: Pergamon)
[2] Kistaiah P, Venudhar Y C, Sathyanarayana Murthy K, Iyengard L and Krishna R K V 1981 *J. Less Common. Met.* **77** 17–9
[3] Jaffe F E and Zunger A 1984 *Phys. Rev.* B **29** 1882
[4] Massushita H, Endo S and Irie T 1991 *Japan. J. Appl. Phys.* **30** 1181
[5] Boyd G D, Kasper H M, MacFee J H and Storz F G 1972 *IEEE J. Quantum. Electron.* **QE-8** 900
[6] Kildal H and Mikkelsen J C 1973 *Opt. Commun.* **9** 315
[7] Byer R L, Choy M M, Herbst R L, Chemla D S and Feigelson R 1974 *Appl. Phys. Lett.* **24** 65
[8] Neumann H 1987 *Cryst. Res. Technol.* **22** 723
[9] Gonzalez J, Calderon E, Tinoco T, Itie J P, Polian A and Moya E 1995 *J. Phys. Chem. Solids* **56** 507
[10] Tinoco T, Polian A, Itie J P, Moya E and Gonzalez J 1995 *J. Phys. Chem. Solids* **56** 481
[11] Neumann H, Horing W, Reccius E, Moller W and Kuhn G 1978 *Solid State Commun.* **27** 449
[12] Arora A, Sakuntala T and Artus L 1993 *J. Phys. Chem. Solids* **54** 381
[13] Choi In-H and Yu P Y 1994 *Solid State Commun.* **90** 345
[14] Calderon E and Gonzalez J 1995 *Cryst. Res. Technol.* **31** 251
[15] Gonzalez J, Fernandez B, Besson J M, Gauthier M and Polian A 1992 *Phys. Rev.* B **46** 15 092
[16] Camassel J, Artus L and Pascual J 1990 *Phys. Rev.* B **41** 5717
[17] Choi In-H and Yu P Y 1994 *Phys. Rev.* B **49** 16 407
[18] Artus L, Pujol J, Pascual J and Camassel J 1990 *Phys. Rev.* B **41** 5727
[19] Worlton T G and Warren J L 1972 *Comput. Phys. Commun.* **3** 88
[20] Eckold G *Unisoft: a Program Package for Lattice Dynamical Calculations: User Manual* 2nd revised edn Jül.Spez-366
[21] Talwar N, Vandzuyver M, Kunc K and Zigone M 1981 *Phys. Rev.* B **24** 741
[22] Weinstein B A 1977 *Solid State Commun.* **24** 595
[23] Deus P, Neumann H, Kuhn G and Hinze B 1983 *Phys. Status Solidi* a **80** 205
[24] Capet F 1995 *Thèse* l'Université de Lille I
[25] Weber W 1977 *Phys. Rev.* B **15** 4789
[26] Musgrave M J P and Pople J A 1962 *Proc. R. Soc.* A **268** 474
[27] Horinaka H, Nozuchi H, Sonomura H and Miyauche T 1983 *Japan. J. Appl. Phys.* **22** 546
[28] Grinsditch M H and Holah G D 1975 *Phys. Rev.* B **12** 4377
[29] Vanne D and Wallace C 1972 *Thermodynamics of Crystals* (New York: Wiley) pp 32–41
[30] Eimerl D, Marion J, Graham E K, Mekinsbry H A and Haussühl S 1991 *IEEE J. Quantum Electron.* **QE-27** 142
[31] Poplavnoi A S and Tjuterev V G 1975 *J. Physique Coll.* **36** C3 169
[32] Lauwers H A and Herman M A 1977 *J. Phys. Chem. Solids* **38** 983